IEEE Photonics Journal
An IEEE Photonics Society Publication

Open Access

Controlled Generation of Bright or Dark Solitons in a Fiber Laser by Intracavity Nonlinear Absorber

Volume 8, Number 3, June 2016

Jun Guo
Yufeng Song
Yuangjiang Xiang
Han Zhang
D. Y. Tang

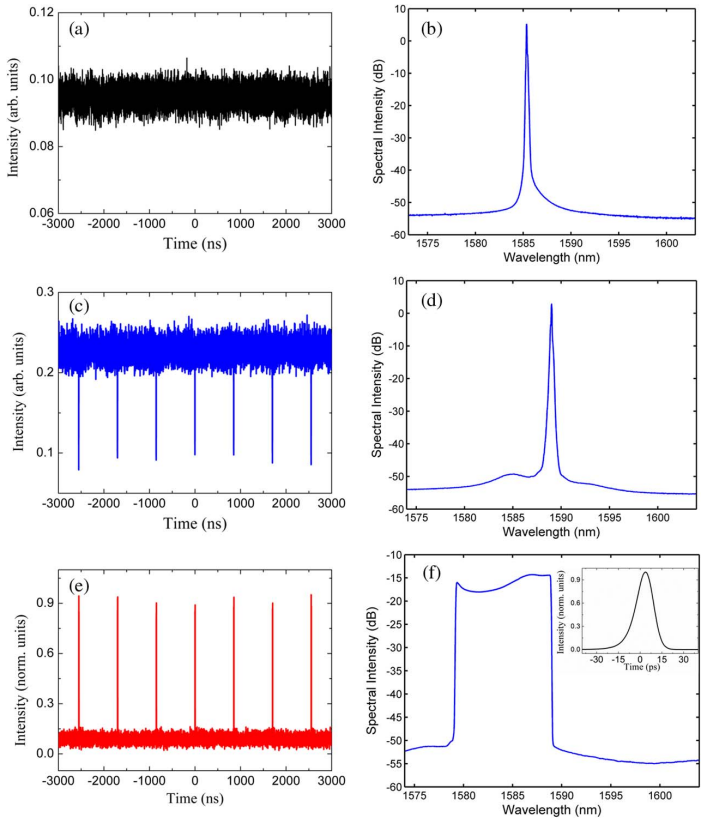

DOI: 10.1109/JPHOT.2016.2575862
1943-0655

IEEE photonics SOCIETY

IEEE

Controlled Generation of Bright or Dark Solitons in a Fiber Laser by Intracavity Nonlinear Absorber

Jun Guo,[1] Yufeng Song,[1] Yuangjiang Xiang,[1] Han Zhang,[1] and D. Y. Tang[2]

[1]Shenzhen University-National University of Singapore Collaborative Innovation Center for Optoelectronic Science and Technology, Key Laboratory of Optoelectronic Devices and Systems of Ministry of Education and Guangdong Province, College of Optoelectronic Engineering, Shenzhen University, Shenzhen 518060, China
[2]School of Electrical and Electronic Engineering, Nanyang Technological University, Singapore 639798

DOI: 10.1109/JPHOT.2016.2575862

Manuscript received March 29, 2016; revised May 25, 2016; accepted May 29, 2016. Date of publication June 14, 2016; date of current version June 17, 2016. This work was supported in part by the National Natural Science Foundation of China under Grant 61505111, Grant 61435010, and Grant 61490713; by the Guangdong Natural Science Foundation under Grant 2015A030313549; by the Science and Technology Planning Project of Guangdong Province under Grant 2016B050501005; by the Science and Technology Project of Shenzhen under Grant JCYJ20140828163633996 and Grant JCYJ20150324141711667; by the Natural Science Foundation of Shenzhen University under Grant 201517, Grant 201452, Grant 827-000051, Grant 827-000052, Grant 282, and Grant 827-000059; and by the Ministry of Education Singapore under Grant 35/12. Corresponding authors: Y. Xiang and H. Zhang (e-mail: xiangyuanjiang@126.com; zhanghanchn@hotmail.com).

Abstract: We numerically found that an intracavity nonlinear absorber (saturable absorber or reversed saturable absorber) plays a crucial role in the formation of dissipative bright or dark solitons in a fiber laser. The operation of an all-normal-dispersion fiber laser could evolve from a bright-soliton emission state to a black-soliton emission state, purely by changing the intracavity nonlinear absorber from a saturable absorber to an antisaturable absorber. Our simulation results are well supported by the experimental observations. The result suggests a new way to control the dissipative soliton operation of lasers and deepens our understanding of the properties of dissipative solitons.

Index Terms: Solitons and polaritons, fiber lasers, fiber nonlinear optics.

1. Introduction

The nonlinear Schrödinger equation (NLSE) admits stable self-localized solutions, known as solitons, both in the positive and negative group velocity dispersion (GVD) regions [1]–[4]. A NLSE soliton has the characteristic that it preserves its amplitude profile during propagation as a result of the balance between dispersion and nonlinearity. While a NLSE soliton formed in the negative GVD region has a bell-shape intensity profile, known as a bright soliton, the ones formed in the positive GVD region display as a sharp intensity dip on a plane-wave background. Such a soliton is known as a dark soliton. The NLSE dark solitons were first experimentally verified by Emplit *et al.* in 1987 [5]. Considering that the NLSE bright and dark solitons form in the complementary GVD regions, it seems impossible that both a bright and a dark soliton form in the same fiber laser with identical configuration.

Stable localized solutions could also be found in equations describing the dynamics of nonlinear dissipative systems. The solitons are called dissipative solitons as in the systems energy intake and dissipation play an important role on the soliton formation. A passively mode-locked fiber laser is a typical dissipative system that admits dissipative soliton formation. In a fiber laser, in addition of the dispersion and nonlinearity, there are linear and nonlinear losses, gain and gain bandwidth filtering, and mode locker, etc., and the mutual interaction and balances among them lead to the formation of dissipative solitons [6]. Different from the NLSE solitons, a dissipative bright soliton can be formed either in the negative GVD or the positive GVD region. The formation of dissipative bright solitons in the positive GVD region of fiber lasers has been intensively studied previously [7]. Moreover, the formation of dark solitons in the positive dispersion fiber lasers was also experimentally confirmed by Sylvestre *et al.* and Zhang *et al.* [8], [9]. It shows that a positive GVD fiber laser is capable of generating either dark solitons or dissipative bright solitons.

Although ubiquitous in a wide range of nonlinear systems such as plasmas and Bose-Einstein condensates, a thorough investigation on the generation and conversion of the bright and dark solitons remained untouched. In addition, from the laser physics point of view, despite of the fact that passive mode locking of lasers has been extensively studied [10], there are still features of the lasers that are not fully understood. Worth of mentioning here that Chouli *et al.* have correlated the existence of soliton rains with the weak mode-locking of a laser [11]; Feng *et al.* reported experimental observation of dark pulses in a mode-lock quantum dot semiconductor laser [12], and Ablowitz *et al.* reported a theoretical model on the dark soliton formation in a mode-locked laser [13]; Schroeder *et al.* reported the generation of bright or dark pulses in a laser as the cavity dispersion is tuned from the negative to positive GVD with the help of a spectral pulse-shaper [14], and Feng *et al.* recently reported the generation of bright or dark pulses in a nonlinear polarization rotation (NPR) mode-locked laser [15]; Zhao *et al.* generated dark pulses and Q-switched pulses in an ytterbium-doped fiber laser [16]; Kelleher *et al.* reported the existence of dark soliton-like structures in ultra-long mode-locked fiber lasers [17]. Is the dark pulse generation related to the mode locking of the lasers? Based on laser physics, the synchronization of longitudinal cavity modes would only give rise to the bright pulses rather than dark pulses [18]. In [17], it is reported that during the dissipative bright solitons' evolution in a mode-locked fiber lasers, a large number of incoherent dark solitons spontaneously emerge from the initial noise. Meanwhile, we also note that dark soliton generation in fiber lasers without mode-locking was also reported [19]–[21].

In studying the dynamics of dissipative solitons, various passive mode-locking techniques have been employed, such as semiconductor saturable absorption mirrors (SESAMs) [22]–[25], nonlinear optical loop mirrors [26]–[28], carbon nanotubes [29]–[31], graphene [32], [33], topological insulator [34], [35], and the nonlinear polarization rotation (NPR) method [36]–[40]. Theoretically the formation of dissipative solitons in mode-locked fiber lasers is modeled by the complex Ginzburg-Landau equation (GLE), which is an extension of the nonlinear Schrödinger equation to include the effects of gain and losses, and the saturable absorption, etc. [41]–[45]. So far, the dissipative bright solitons have been extensively investigated and dissipative dark soliton in plasma was also discussed in [46], while the formation of dissipative dark solitons in fiber lasers has not been addressed. In this paper, based on the operation of an all-normal dispersion fiber laser that has a typical NPR mode locking cavity configuration, we numerically show that depending on the setting of the linear cavity phase delay bias (LCPDB), the same laser could operate in different modes: either in CW emission, dark soliton emission, or bright soliton emission. In a NPR mode locking fiber laser the LCPDB is changeable through turning the orientation of the intra-cavity polarization controller. It is now well known that in fiber lasers, the combined action of the NPR of light in the cavity and an intracavity polarizer could lead to the formation of an artificial nonlinear optical absorber, and depending on the setting of the LCPDB, this artificial absorber could have either weak or strong saturable absorption (SA) or reversed saturable absorption (RSA), respectively [47]. We show numerically that the different modes of the laser operation are related to the different features of the artificial absorber.

2. Results of Numerical Simulations

In a previous paper [48], we proposed a technique to numerically faithfully simulate the operation of a NPR mode locking fiber laser. Here we will base on an actual fiber laser configuration to highlight the technique. Generally, we start the numerical simulation with an arbitrary weak light signal. We let the light propagate in the laser cavity. The light propagation in the weak birefringent cavity fibers is described by the coupled complex Ginzburg-Landau equations (GLEs)

$$\frac{\partial u}{\partial z} = i\beta u - \delta\frac{\partial u}{\partial t} - \frac{ik''}{2}\frac{\partial^2 u}{\partial t^2} + \frac{k'''}{6}\frac{\partial^3 u}{\partial t^3} + i\gamma\left(|u|^2 + \frac{2}{3}|v|^2\right)u + \frac{i\gamma}{3}v^2u^* + \frac{g}{2}u + \frac{g}{2\Omega_g^2}\frac{\partial^2 u}{\partial t^2}$$
$$\frac{\partial v}{\partial z} = -i\beta v + \delta\frac{\partial v}{\partial t} - \frac{ik''}{2}\frac{\partial^2 v}{\partial t^2} + \frac{k'''}{6}\frac{\partial^3 v}{\partial t^3} + i\gamma\left(|v|^2 + \frac{2}{3}|u|^2\right)v + \frac{i\gamma}{3}u^2v^* + \frac{g}{2}v + \frac{g}{2\Omega_g^2}\frac{\partial^2 v}{\partial t^2} \quad (1)$$

$$g = \begin{cases} g = G\exp\left[-\int |u|^2\, dt/E_{\text{sat}}\right], & \text{for erbium doped fiber} \\ 0, & \text{others} \end{cases} \quad (2)$$

where u and v are the envelopes of the light along the two orthogonal polarization axes of the cavity fibers. $\beta = \pi/L_b = \pi\Delta n/\lambda$ accounts for the birefringence, and L_b is the beat length. The group velocity mismatch is given by $\sigma = \beta\lambda/2\pi c$. The second and third order dispersion coefficients are given by k'' and k''', respectively, γ is the nonlinear coefficient. g is the saturable gain coefficient, and Ω_g is the spectral bandwidth of the gain. For a non-doped fiber $g = 0$. Gain saturation of the doped fiber is considered by equation (2), where G is the small signal gain, and E_{sat} is the gain saturation energy.

We used the standard split-step Fourier method to solve the GLEs. To this end a simulation window with a length of 100 ps together with the periodic boundary condition is used. We model the cavity components, such as the output coupler and intracavity polarizer, with their transfer matrix. Whenever the light meets an intracavity component, we multiply the light with the transfer matrix of the component. After one roundtrip of the light propagation in the cavity, we then use the final result of the light field as the input for the next roundtrip calculation. The procedure will repeat until a steady state is obtained. We consider that the steady state obtained is one of the possible laser operation states experimentally observed. With the technique we have reproduced almost all the experimental phenomena observed in our fiber lasers, including the dissipative soliton formation and the dark soliton formation [8], [25].

We will consider a fiber laser with the following cavity configuration: the fiber cavity is made of two types of optical fibers: 5 m erbium doped fiber (EDF) with a GVD parameter of –32 (ps/nm)/km and a total length of 170 m dispersion compensation fiber (DCF) with a GVD parameter of –4 (ps/nm)/km, and the orientation of the intra-cavity polarizer (analyzer) to the fast axis of the weakly birefringent fiber: $\theta = 0.125\pi$, $\varphi = \pi/2 + \theta$; the nonlinear fiber coefficient $\gamma = 3\ \text{W}^{-1}\text{km}^{-1}$; EDF gain bandwidth $\Omega_g = 16$ nm; fiber dispersions: $k''_{\text{DCF}} = 5.2\ \text{ps}^2/\text{km}$, $k''_{\text{EDF}} = 41.6\ \text{ps}^2/\text{km}$, $k''' = -0.13\ \text{ps}^3/\text{km}$, cavity output ratio $= 10\%$, and $E_{\text{sat}} = 500$ pJ, and the linear cavity birefringence is $L/L_b = 0.05$.

We have numerically studied the operation of the above fiber laser under various LCPDBs: $\Delta\varphi_b$. To possibly excite complicate laser dynamics we have fixed the small signal gain coefficient at $G = 3000\ \text{km}^{-1}$ in our simulations. Fig. 1 shows the laser operation mode change with the LCPDB settings numerically obtained. It shows that through simply varying the LCPDB the laser operation could be switched from CW operation to the black soliton emission, to the dissipative soliton emission, and back to CW emission. Fig. 2 further illustrates the typical temporal and spectral profiles of the laser emission under different operation modes. When the LCPDB is selected in the range from 0.1π to 0.7π, the laser emits in a CW state, as shown in Fig. 2(a) and (d). When LCPDB is in the range of 0.8π to 1.03π, the laser operates in a black soliton emission state, as shown in Fig. 2(b) and (e). The black solitons have a pulse width of ~3.1 ps, and a 3 dB spectral bandwidth of 0.3 nm. However, as the LCPDB becomes larger than 1.03π, the fiber laser operation switches to the dissipative bright soliton emission state, as shown in Fig. 2(c) and (f). The

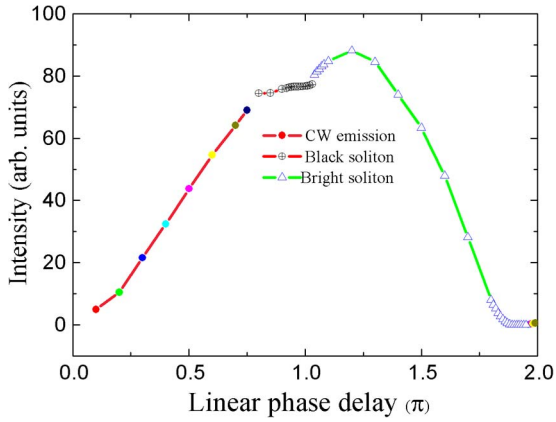

Fig. 1. Numerically calculated laser output intensity change with LCPDB. With other parameters kept constant, the laser emission state varied from a CW ($\Delta\varphi_b$: $0.1\pi \sim 0.7\pi$), to a black soliton ($\Delta\varphi_b$: $0.8\pi \sim 1.03\pi$), to a dissipative bright soliton ($\Delta\varphi_b$: $1.04\pi \sim 1.95\pi$), and then back to a CW ($\Delta\varphi_b$: $1.96\pi \sim 2.0\pi$) emission state.

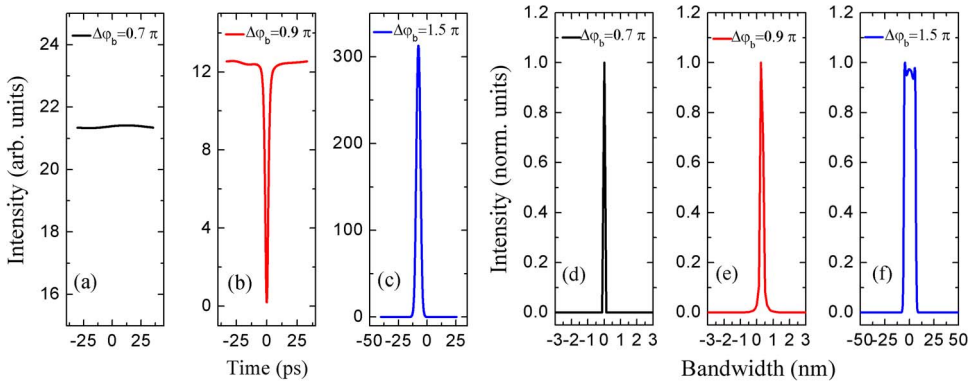

Fig. 2. Numerically calculated temporal and spectral profiles of the laser emission under different LCPDBs. (a) and (d) CW state ($\Delta\varphi_b = 0.7\pi$). (b) and (e) Dissipative black-soliton state ($\Delta\varphi_b = 0.9\pi$). (c) and (f) Dissipative bright-soliton state ($\Delta\varphi_b = 1.5\pi$).

spectrum of the laser emission has the characteristic steep spectral edges with a 3 dB spectral bandwidth of 15.3 nm. The dissipative bright soliton has a pulse width (FWHM) of 2.4 ps. The time-bandwidth product of the pulses is about 4.59, indicating that they are chirped solitons. Further increasing the LCPDB from 1.04π, the output intensity of the laser will grow slowly until $\Delta\varphi_b = 1.2\pi$. Afterward it gradually decreases, as shown in Fig. 1. Eventually, a broad bright pulse with low intensity is obtained at $\Delta\varphi_b = 1.9\pi$. If LCPDB is further increased from 1.95π to 2.0π, the laser emission is again CW.

The dissipative bright soliton operation of the fiber laser has been extensively investigated, and the features of the laser operation are well understood. Therefore, we will focus on the dark soliton operation of the fiber laser. It is numerically found that as the LCPDB $(\Delta\varphi_b)$ is set in the range of $0.8\pi \sim 0.97\pi$, a single black soliton is always obtained. Moreover, the black soliton obtained under different LCPDBs has nearly identical soliton parameters: the pulse width remains ~3.1 ps which is independent on the LCPDB change. In the range of $0.98\pi \sim 1.03\pi$, the single black soliton is no longer stable. It breaks up into multiple black solitons.

We emphasize that the different modes of laser operation are the intrinsic feature of the laser under the particular LCPDB setting. This feature of the fiber laser enables the conversion of a bright dissipative soliton to a black one and *vice versa* in the same laser. To demonstrate it, we

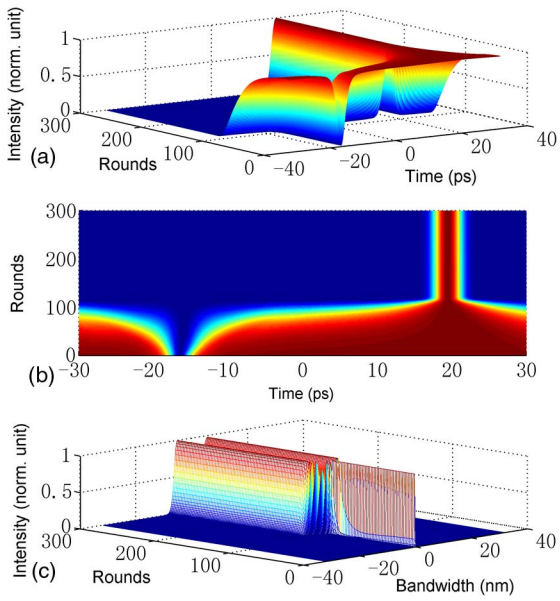

Fig. 3. Conversion of a dissipative black soliton into a bright soliton. LCPDB $= 1.7\pi$. (a) and (b) Temporal evolutions. (c) Spectral evolution.

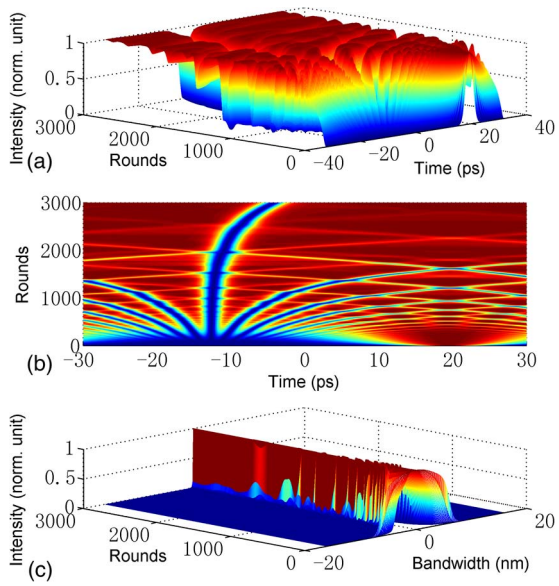

Fig. 4. Conversion of a dissipative bright soliton into a black soliton. LCPDB $= 0.9\pi$. (a) and (b) Temporal evolutions. (c) Spectral evolution.

have numerically simulated the operation of our fiber laser initially at the LPCDB $= 0.9\pi$, where a stable black soliton with a pulse width of 3.1 ps and 3 dB bandwidth of 0.3 nm is formed. We then adjusted the cavity LCPDB to 1.7π with the black soliton as the input. The black soliton is quickly reshaped to a dissipative bright soliton after only 100 rounds, as is shown in Fig. 3. When we do it reversely, after 2500 rounds, a stable bright pulse with pulse width of 2.4 ps and 3 dB bandwidth of 15.3 nm is shaped into a black soliton with a pulse width of 3.1 ps and spectral bandwidth of 0.3 nm, as shown in Fig. 4. The result also indicates that in the fiber laser a bright soliton state is much easier to obtain than a black soliton state.

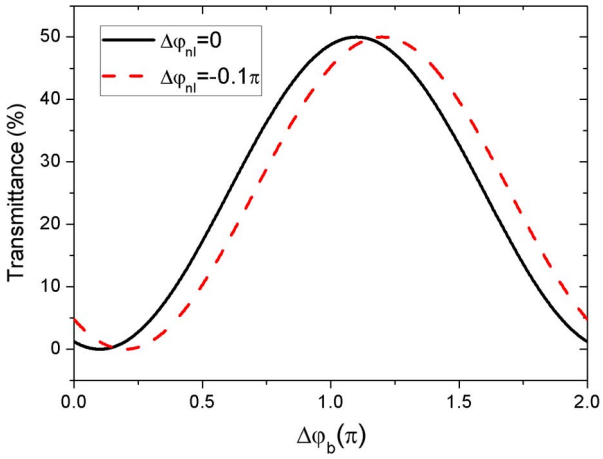

Fig. 5. (Black solid) Linear and (red dashed) nonlinear cavity transmission of the numerically simulated fiber laser with the LCPDB.

3. Discussion

The numerical simulations clearly show that in the same fiber laser, depending on the LCPDB setting either the bright dissipative soliton emission or the black soliton emission could be obtained. Previous studies have shown that the formation of the bright dissipative solitons is related to the passive mode locking of the fiber laser. Due to the existence of the artificial saturable absorber in the cavity under the particular LCPDB setting, passive mode locking occurs in the laser. Mode locking results in the formation of strong optical pulses. The nonlinear shaping of the pulses in the cavity further turns the pulses into dissipative bright solitons. However, the formation mechanism of the black solitons in the fiber laser is not clear. Based on the NLSE it is expected that dark solitons should be able to be formed in an all-normal dispersion cavity fiber laser, but why only in a certain LCPDB setting could the black solitons be formed? What is the role played by the gain and the nonlinear absorber in the fiber laser? All these questions are still unclear. To answer the questions, we further studied the relation of the LCPDB settings to the artificial saturable absorber formed in the cavity.

We note that the cavity transmission of a fiber laser with the NPR mode locking configuration is determined by [47]

$$T = \sin^2(\theta)\sin^2(\varphi) + \cos^2(\theta)\cos^2(\varphi) + \frac{1}{2}\sin(2\theta)\sin(2\varphi)\cos(\Delta\varphi_l + \Delta\varphi_b + \Delta\varphi_{nl}) \quad (3)$$

where θ and φ are the angle of the intracavity polarizer (analyzer) formed with respect to the fast axis of the cavity birefringence, $\Delta\varphi_l$ is the linear cavity phase delay due to the fiber birefringence, $\Delta\varphi_b$ is the LCPDB, and $\Delta\varphi_{nl}$ is the nonlinear cavity phase delay (NCPD) caused by the light propagation over one roundtrip in the cavity. With the θ, φ fixed at the values used in the simulation, the linear cavity transmission coefficient with the LCPDB is shown in Fig. 5. Considering that the NCPD is negative and generally is a very small value, we have also draw the cavity transmission curve under existence of a weak NCPD in the same figure. It becomes clear that depending on the LCPDB setting, under existence of NPR the nonlinear cavity transmission would either increase with the light intensity or decrease with it, or in another word, the artificial intracavity absorber could either behave as a saturable absorber or a reverse saturable absorber. Specifically, in the range of LCPDB from 0.1π to 1.03π, it is an anti-saturable absorber, while in the range of 1.04π to 2π it is a SA. The result suggests that the black soliton generation is related to the reverse saturable absorber.

Because the saturable and reverse saturable absorption of the artificial absorber is implied by (3), it is difficult to clearly see their effects on the dark or bright soliton formation, and full

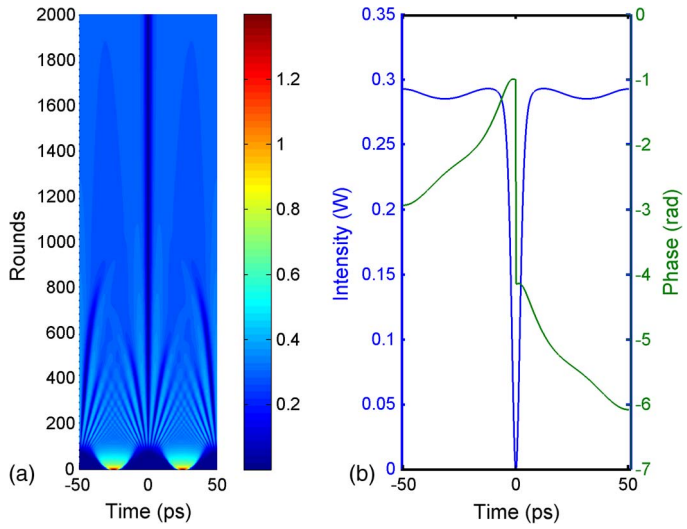

Fig. 6. (a) Effect of RSA on two bright pulses. (b) Intensity and phase profile after 2000 round trips propagation.

simulations like Fig. 3 are time consuming, which is difficult to calculate with large parameter space. Therefore, in the following simulation, we use an averaged mode which can be calculated much faster to study how SA or RSA works in our fiber lasers. It should be noticed that the following simulation is mainly for illustration purpose, so the cavity parameters are not necessarily matched with experimental parameters, not like that in Figs. 3 and 4, and we have also calculated with different parameters to make sure that we can get similar results. According to [48], a fiber laser mode locked by NPR method can be reduced to a quintic complex GLE. So to make the artificial absorber's effects straightforward, we further use the averaged equation model of the fiber laser [49]

$$i\frac{\partial u}{\partial z}-\frac{\beta_2}{2}\frac{\partial^2 u}{\partial t^2}+\gamma|u|^2u-i\frac{g}{2}u-i\frac{g}{2\Omega_g^2}\frac{\partial^2 u}{\partial t^2}=i\varepsilon|u|^2u+i\mu|u|^4u. \tag{4}$$

The parameters used in the equation have the same meanings as those used in (1), however, it is to bear in mind that they are averaged over the cavity length. The first term on the right hand represents the artificial SA if ε is positive, and the second term represents the artificial RSA caused by overdriven of effective SA if μ is negative. The values of ε and μ can be set to be arbitrary values according to [49]. We used the following parameters for the simulation: the cavity length is 20 m, the nonlinear fiber coefficient $\gamma = 3\ \mathrm{W^{-1}km^{-1}}$; gain bandwidth $\Omega_g = 40$ nm; averaged fiber dispersions: $\beta_2 = 6.24\ \mathrm{ps^2/km}$, the cavity output $= 10\%$, $E_{\mathrm{sat}} = 6.6$ pJ.

First we set $\varepsilon = 3\ \mathrm{W^{-1}km^{-1}}$ and $\mu = -9\ \mathrm{W^{-2}km^{-1}}$, with these values the dominant artificial absorber is RSA. In our simulations we start with an initial condition that is two bright pulses similar to that in Fig. 4. Due to the period boundary condition used in our simulations, these two initial pulses, in fact, represent a pulse train with repetition of 40 GHz, and our previous works have proved that even without mode-locked components stable pulse trains still exist in fiber lasers [20], [50]. Therefore, such initial situation can be realized in practice. The results are shown in Fig. 6, we show the evolution of two initial bright pulses in Fig. 6(a) and intensity and phase profile after 2000 round trips propagation. As can be seen, similar to Fig. 4, two bright pulses quickly vanish and several grey pulses and one black pulse appear in the subsequent cavity round trips. However, due to the effect of RSA the grey pulses could not become grey solitons. They eventually vanish after hundreds of cavity roundtrips. On the contrary, the black pulse is hardly affected by the RSA. Comparing Fig. 6 with Fig. 4, it is easy to understand why when LCPDB $= 0.9\pi$, a black soliton was formed in the numerical simulation. We can tell that the

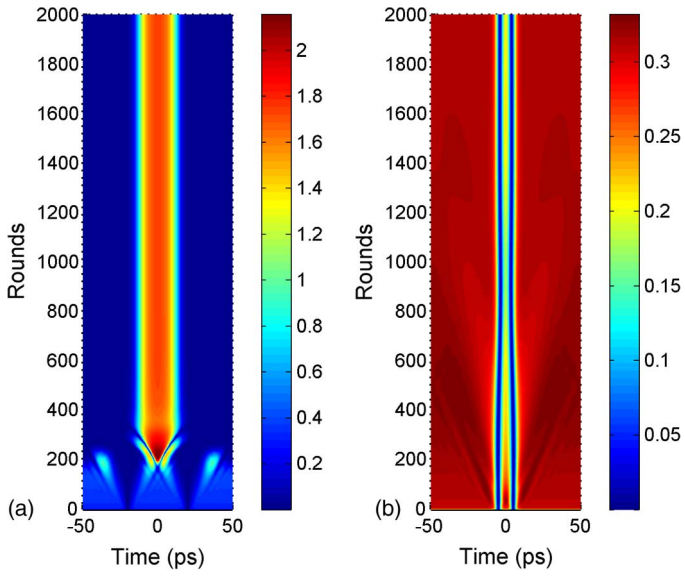

Fig. 7. (a) Effects of SA on two black pulses. (b) Effects of RSA on two adjacent black pulses.

seed of black solitons are interference between two pulses while the stabilization and selection of black solitons are contributed by RSA. We stress that the RSA can suppress all gray solitons' formation in the cavity, only black solitons can exists, i.e. a selection function. Without RSA, the formation of dark solitons are thresholdless and gray solitons with different depth, width and also velocity will coexist and make the output of lasers too complex to be analyzed [51]. We also show the phase profile of the black pulse after 2000 round trips propagation, we can see clearly that there is π phase jump which indicates the resulted black pulse is black soliton.

We then set $\varepsilon = 3\ \mathrm{W^{-1}km^{-1}}$ and $\mu = -0.9\ \mathrm{W^{-2}km^{-1}}$; with these values, the dominant artificial absorber is SA. We start the simulation with two black pulses. We set large values of ε to simulate the strong mode-locking region. The result in Fig. 7(a) is similar to that of Fig. 3, indicating that when LCPDB $= 1.7\pi$, the NPR is equivalent to a strong SA. With strong SA the black pulses vanish fast, and a new bright pulse is obtained. The bright pulse keeps its shape and can be regarded as a bright soliton.

Finally we set $\varepsilon = 3\ \mathrm{W^{-1}km^{-1}}$ and $\mu = -5.4\ \mathrm{W^{-2}km^{-1}}$, the RSA is still dominant while have smaller value. Different with Fig. 6, we start the simulation with two adjacent black pulses. We get interesting results shown in Fig. 7(b). We can see in Fig. 7(b) that two adjacent black pulses attract each other and finally form a stable bound state. Such bound state was predicted in [51] and is a natural results of quintic CGLE with certain values of ε and μ. The resulted intensity profile shows clearly the bound state form like in [52]. This simulation result may explain why in our experiments black pulses with large width are always obtained, which will be discussed in the following part. Above all, the simulation results could well explain the formation of different soliton states and their relation to the features of the intracavity nonlinear absorber.

4. Experimental Observations

Our numerical simulations show that as the LCPDB is changed, a NPR configuration fiber laser could switch from a black soliton emission state to a bright dissipative soliton emission state, and the physical mechanism behind it is the intracavity artificial absorber changed from a reverse saturable absorber to a saturable absorber. To confirm the numerical results, we constructed an erbium-doped fiber ring laser with the NPR cavity configuration [8] and experimentally investigated its operation. To possibly match the conditions of numerical simulations, the fiber cavity was made with 5 m normal dispersion EDF that has a group velocity

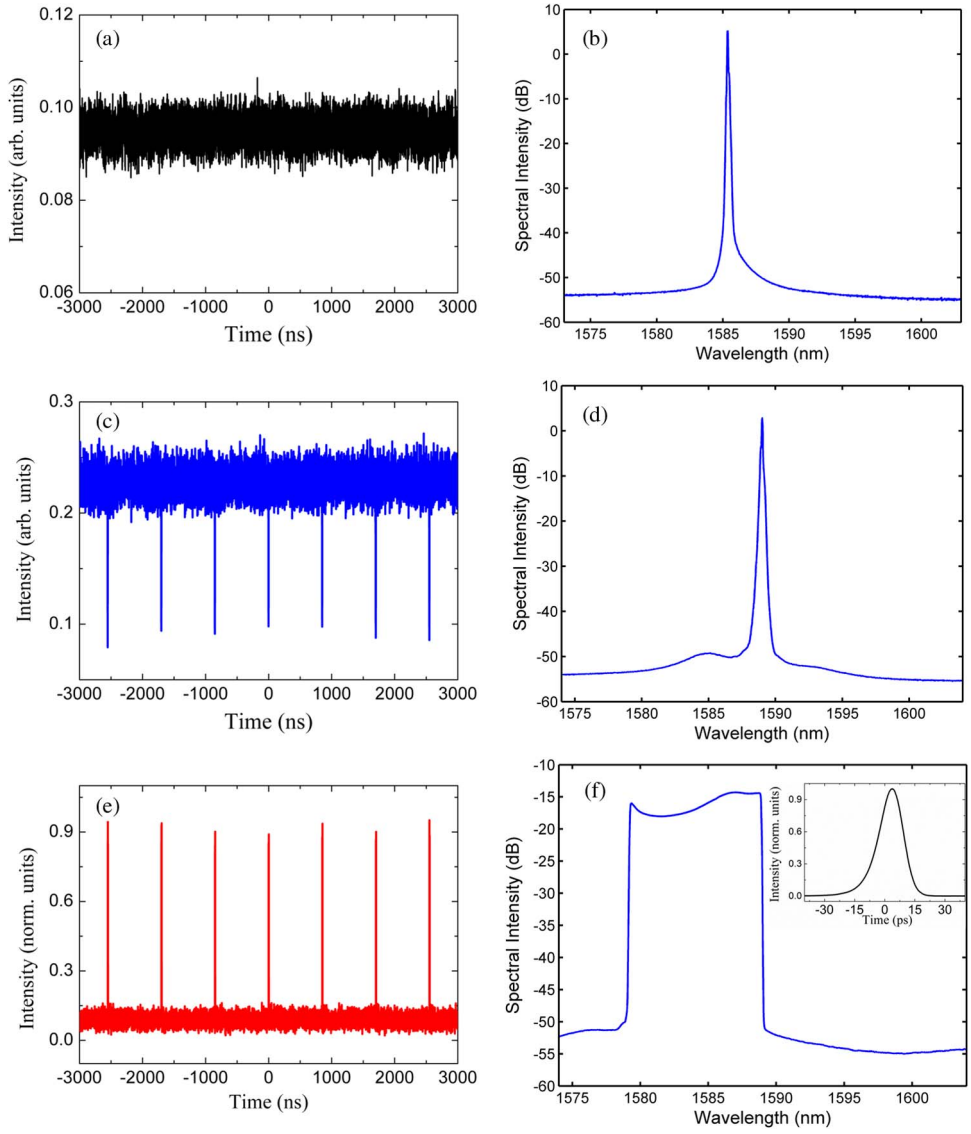

Fig. 8. Different laser emission states experimentally observed. (Left column) Oscilloscope traces. (Right column) Optical spectra. (a) and (b) CW state. (c) and (d) Dissipative dark soliton state. (e) and (f) Dissipative bright-soliton state. The autocorrelation trace of the dissipative bright solitons is also given in the inset in (f).

dispersion parameter of –32 ps/nm/km and a total length of 170 m DCF that has a GVD parameter of –4 ps/nm/km. A polarization dependent isolator was inserted in the cavity to force the unidirectional operation of the fiber ring. The polarization dependent isolator also acted as an intracavity polarizer, forming together with the fiber ring cavity an artificial absorber in the cavity. An in-cavity polarization controller (PC) was used in the cavity to fine tune the linear cavity birefringence, thus changes the LCPDB. A fiber coupler with an output ratio of 10' was used to emit the optical signal, and the laser is pumped by a high power Fiber Raman Laser source of wavelength 1480 nm with maximum pump power up to 5 W. The emission of the laser cavity was simultaneously monitored by an optical spectrum analyzer and a 5 GHz oscilloscope together with a 2 GHz photo-detector. A commercial auto-correlator was used to measure the pulse width of the dissipative solitons.

The total cavity dispersion is estimated 1.092 ps^2/km. We operated the fiber laser at an intracavity power of ~300 mW. Experimentally it was found that by solely changing the orientations of the intracavity polarization controller, three different emission states as shown in the numerical simulations could always be obtained. Fig. 8 shows the three typical laser emission states experimentally observed. At an appropriate LCPDB setting the self-started mode locking of the fiber laser was achieved. After the mode locking, the laser then emitted a stable train of bright pulses. The pulses repeated with the fundamental cavity repetition rate. The autocorrelation measurement, as shown in the insert of Fig. 8(f), shows that the pulses have a pulse width of ~8.4 ps. As the optical spectra of the pulses have the typical characteristics of the dissipative bright solitons, the state is identified as a dissipative soliton emission state. Fixing all the other laser parameters but only tuning the LCPDB, the laser emission could be switched to a stable dark pulse emission state, as shown in Fig. 8(b). The dark pulse had broad pulse width and repeated with the cavity repetition rate. Detailed experimental studies have shown that the broad dark pulse is actually a bunching of many dark solitons formed in the fiber laser [53], [54]. Under strong pumping many dark pulses were simultaneously formed in the cavity. Under effect of the reverse saturable absorber the dark solitons have the tendency of bunching together. Consequently they form a giant dark pulse in the cavity and move with the cavity repetition rate as shown. The dark soliton feature of the pulses is also characterized by the soliton sidebands formation on their optical spectra, as shown in Fig. 8(d). It was a result of the constructive interference between dark solitons and dispersive waves when they co-propagate inside the laser cavity [55]. The experimental observation well confirms the numerical simulations.

5. Conclusion

It was experimentally shown that apart from the bright dissipative soliton emission, a normal dispersion cavity fiber laser can also emit black solitons. Based on numerical simulations we found that the black soliton formation in the fiber laser is a result of the artificial anti-saturable absorber formed in the cavity. By changing the LCPDB the formed artificial saturable absorber could be changed to an anti- saturable absorber, which leads to that the fiber laser emission switches from a dissipative bright soliton emission state to a dissipative dark solitons emission state.

The dark soliton formation is an intrinsic feature of the strong light propagation in the normal dispersion single mode fibers. Different from the bright soliton formation, the dark soliton formation is thresholdless [21], [56]. Any intensity or phase noise could result in dark soliton formation. As a result of this thresholdless feature generally dark solitons with different darkness and pulse width would be formed. However, our numerical simulation shows that if there is an anti-saturable absorber in the system, under effect of the anti-saturable absorber only the black solitons are stable. Moreover, the effect of an anti-saturable absorber on the dark pulses is similar to that of a saturable absorber on the bright pulses. It generates a kind of attraction force between the dark pulses. Therefore, the dark solitons formed in a NPR configuration fiber laser always bunch together, forming a giant dark pulse. On the other hand, a dissipative dark soliton is unstable under existence of a saturable absorber in the system. A saturable absorber could cause mode locking of a laser. This was why under effect of an artificial saturable absorber dissipative bright solitons were formed in our fiber laser. Based on our numerical simulations we could now answer the questions raised in the introduction part. The dark soliton formation in a fiber laser actually requires no mode locking. In fact an anti-saturable absorber has no mode locking function. Its function is to select the black solitons and drive them together to form a giant black pulse.

References

[1] L. F. Mollenauer, R. H. Stolen, and J. P. Gordon, "Experimental observation of picosecond pulse narrowing and solitons in optical fibers," *Phys. Rev. Lett.*, vol. 45, p. 1095, 1980.

[2] Y. S. Kivishar and G. Agrawal, *Optical Solitons: From Fiber to Photonic Crystals*. San Diego, CA, USA: Academic, 2003.

[3] Y. S. Kivshar and B. Luther-Davies, "Dark optical solitons: Physics and applications," *Phys. Rep.*, vol. 298, no. 2/3, pp. 81–197, May 1998.
[4] L. M. Zhao, D. Y. Tang, and J. Wu, "Gain-guided soliton in a positive group-dispersion fiber laser," *Opt. Lett.*, vol. 31, no. 12, pp. 1788–1790, 2006.
[5] P. Emplit, J. P. Hamaide, F. Reynaud, C. Froehly, and A. Barthelemy, "Picosecond steps and dark pulses through nonlinear single mode fibers," *Opt. Commun.*, vol. 62, no. 6, pp. 374–379, Jun. 1987.
[6] N. Akhmediev and A. Ankievicz, *Dissipative Solitons, From Optics to Biology and Medicine*. Berlin, Germany: Springer-Verlag, 2008.
[7] P. Grelu, W. Chang, A. Ankiewicz, J. M. Soto-Crespo, and N. Akhmediev, "Dissipative soliton resonance as a guideline for high-energy pulse laser oscillators," *J. Opt. Soc. Amer. B*, vol. 27, no. 11, pp. 2336–2341, 2010.
[8] H. Zhang, D. Y. Tang, L. M. Zhao, and X. Wu, "Dark pulse emission of a fiber laser," *Phys. Rev. A*, vol. 80, no. 4, pp. 3383–3387, Oct. 2009.
[9] T. Sylvestre, S. Coen, P. Emplit, and M. Haelterman, "Self-induced modulational instability laser revisited: Normal dispersion and dark-pulse train generation," *Opt. Lett.*, vol. 27, no. 7, pp. 482–484, 2002.
[10] H. A. Haus, "Theory of mode locking with a fast saturable absorber," *J. Appl. Phys.*, vol. 46, no. 7, pp. 3049–3058, 1975.
[11] S. Chouli and P. Grelu, "Soliton rains in a fiber laser: An experimental study," *Phys. Rev. A*, vol. 81, no. 6, 2010, Art. no. 063829.
[12] M. Feng, K. L. Silverman, R. P. Mirin, and S. T. Cundiff, "Dark pulse quantum dot diode laser," *Opt. Exp.*, vol. 18, no. 13, pp. 13385–13395, 2010.
[13] M. J. Ablowitz, T. P. Horikis, S. D. Nixon, and D. J. Frantzeskakis, "Dark solitons in mode locked lasers," *Opt. Lett.*, vol. 36, no. 6, pp. 793–795, 2011.
[14] J. B. Schroeder, S. Coen, T. Sylvestre, and B. J. Eggleton, "Dark and bright pulse passive mode-locked laser with in-cavity pulse-shaper," *Opt. Exp.*, vol. 18, no. 22, pp. 22715–22721, Oct. 2010.
[15] Z. Feng, Q. Rong, X. Qiao, Z. Shao, and D. Su, "Experimental observation of different soliton types in a net-normal group-dispersion fiber laser," *Appl. Opt.*, vol. 53, no. 27, pp. 6237–6242, Sep. 2014.
[16] J. Zhao *et al.,* "An Ytterbium-doped fiber laser with dark and Q-switched pulse generation using graphene-oxide as saturable absorber," *Opt. Commun.*, vol. 312, pp. 227–232, Feb. 2014.
[17] E. J. Kelleher and J. C. Travers, "Chirped pulse formation dynamics in ultra-long mode-locked fiber lasers," *Opt. Lett.*, vol. 39, no. 6, pp. 1398–1401, Mar. 2014.
[18] O. Svelto, *Principles of Lasers*, 3rd ed. New York, NY, USA: Plenum, 1989.
[19] T. Sylvestre, S. Coen, P. Emplit, and M. Haelterman, "Self-induced modulational instability laser revisited: Normal dispersion and dark-pulse train generation," *Opt. Lett.*, vol. 27, no. 7, pp. 482–484, Apr. 2002.
[20] Y. F. Song, J. Guo, L. M. Zhao, D. Y. Shen, and D. Y. Tang, "280 GHz dark soliton fiber laser," *Opt. Lett.*, vol. 39, no. 12, pp. 3484–3487, Jun. 2014.
[21] D. Y. Tang, J. Guo, Y. F. Song, H. Zhang, L. M. Zhao, and D. Y. Shen, "Dark soliton fiber lasers," *Opt. Exp.*, vol. 22, no. 16, pp. 19831–19837, 2014.
[22] M. J. Lederer, B. Luther-Davies, H. H. Tan, C. Jagadish, N. N. Akhmediev, and J. M. Soto-Crespo, "Multipulse operation of a Ti: Sapphire laser mode locked by an ion-implanted semiconductor saturable-absorber mirror," *J. Opt. Soc. Amer. B*, vol. 16, no. 6, pp. 895–904, 1999.
[23] A. Cabasse, G. Martel, and J. L. Oudar, "High power dissipative soliton in an erbium-doped fiber laser mode-locked with a high modulation depth saturable absorber mirror," *Opt. Exp.*, vol. 17, no. 12, pp. 9537–9542, Jun. 2009.
[24] C. Lecaplain, B. Ortaç, and A. Hideur, "High-energy femtosecond pulses from a dissipative soliton fiber laser," *Opt. Lett.*, vol. 34, no. 23, pp. 3731–3733, 2009.
[25] H. Zhang, D. Y. Tang, L. M. Zhao, X. Wu, and H. Y. Tam, "Dissipative vector solitons in a dispersion-managed cavity fiber laser with net positive cavity dispersion," *Opt. Exp.*, vol. 17, no. 2, pp. 455–460, 2009.
[26] L. Yun, X. M. Liu, and D. Mao, "Observation of dual-wavelength dissipative solitons in a figure-eight erbium-doped fiber laser," *Opt. Exp.*, vol. 20, no. 19, pp. 20992–20997, 2012.
[27] S. K. Wang, Q. Y. Ning, A. P. Luo, Z. B. Lin, Z. C. Luo, and W. C. Xu, "Dissipative soliton resonance in a passively mode-locked figure-eight fiber laser," *Opt. Exp.*, vol. 21, no. 2, pp. 2402–2407, 2013.
[28] L. Yun and X. M. Liu, "Generation and propagation of bound-state pulses in a passively mode-locked figure-eight laser," *IEEE Photon. J.*, vol. 4, no. 2, pp. 512–519, Apr. 2012.
[29] X. Liu *et al.,* "Versatile multi-wavelength ultrafast fiber laser mode-locked by carbon nanotubes," *Sci. Rep.*, vol. 3, p. 2718, 2013.
[30] J. H. Im, S. Y. Choi, F. Rotermund, and D. Yeom, "All-fiber Er-doped dissipative soliton laser based on evanescent field interaction with carbon nanotube saturable absorber," *Opt. Exp.*, vol. 18, no. 21, pp. 22141–22146, Oct. 2010.
[31] C. Zeng, X. Liu, and L. Yun, "Bidirectional fiber soliton laser mode-locked by single-wall carbon nanotubes," *Opt. Exp.*, vol. 21, no. 16, pp. 18937–18942, Aug. 2013.
[32] J. Xu *et al.,* "Dissipative soliton generation from a graphene oxide mode-locked Er-doped fiber laser," *Opt. Exp.*, vol. 20, no. 21, pp. 23653–23658, 2012.
[33] J. Sotor, G. Sobon, and K. M. Abramski, "Scalar soliton generation in all-polarization-maintaining, graphene mode-locked fiber laser," *Opt. Lett.*, vol. 37, no. 11, pp. 2166–2168, Jun. 2012.
[34] C. Chi, J. Lee, J. Koo, and J. H. Lee, "All-normal-dispersion dissipative-soliton fiber laser at 1.06 μm using a bulk-structured Bi2Te3 topological insulator-deposited side-polished fiber," *Laser Phys.*, vol. 24, no. 10, 2014, Art. no. 105106.
[35] J. Boguslawski, G. Sobon, R. Zybala, and J. Sotor, "Dissipative soliton generation in Er-doped fiber laser mode-locked by Sb2Te3 topological insulator," *Opt. Lett.*, vol. 40, no. 12, pp. 2786–2789, Jun. 2015.
[36] X. H. Feng, H. Y. Tam, and P. K. A. Wai, "Stable and uniform multiwavelength erbium-doped fiber laser using nonlinear polarization rotation," *Opt. Exp.*, vol. 14, no. 18, pp. 8205–8210, Sep. 2006.

[37] A. D. Kim, J. N. Kutz, and D. J. Muraki, "Pulse-train uniformity in optical fiber lasers passively mode-locked by nonlinear polarization rotation," *IEEE J. Quantum. Elect.*, vol. 36, no. 4, pp. 465–471, Apr. 2000.
[38] X. Fu and J. N. Kutz, "High-energy mode-locked fiber lasers using multiple transmission filters and a genetic algorithm," *Opt. Exp.*, vol. 21, no. 5, pp. 6526–6537, Mar. 2013.
[39] S. Smirnov, S. Kobtsev, S. Kukarin, and A. Ivanenko, "Three key regimes of single pulse generation per round trip of all-normal-dispersion fiber lasers mode-locked with nonlinear polarization rotation," *Opt. Exp.*, vol. 20, no. 24, pp. 27447–27453, Nov. 2012.
[40] L. N. Duan, X. M. Liu, D. Mao, L. R. Wang, and G. X. Wang, "Experimental observation of dissipative soliton resonance in an anomalous-dispersion fiber laser," *Opt. Exp.*, vol. 20, no. 1, pp. 265–270, Jan. 2012.
[41] P. Grelu and N. Akhmediev, "Dissipative solitons for mode-locked lasers," *Nature Photon.*, vol. 6, no. 2, pp. 84–92, Feb. 2012.
[42] J. M. Soto-Crespo, N. Akhmediev, and V. Afanasjev, "Stability of the pulse-like solutions of the quintic complex Ginzburg-Landau equation," *J. Opt. Soc. Amer. B*, vol. 13, no. 7, pp. 1439–1449, 1996.
[43] I. S. Aranson and L. Kramer, "The world of the complex Ginzburg-Landau equation," *Rev. Mod. Phys.*, vol. 74, no. 1, pp. 99–143, Jan.–Mar. 2002.
[44] J. N. Kutz, "Mode-locked soliton lasers," *SIAM Rev.*, vol. 48, no. 4, pp. 629–678, Dec. 2006.
[45] J. M. Soto-Crespo, M. Grapinet, P. Grelu, and N. Akhmediev, "Bifurcations and multiple-period soliton pulsations in a passively mode-locked fiber laser," *Phys. Rev. E*, vol. 70, no. 6, 2004, Art. no. 066612.
[46] R. Heidemann, S. Zhdanov, R. Sütterlin, H. M. Thomas, and G. E. Morfill, "Dissipative dark soliton in a complex plasma," *Phys. Rev. Lett.*, vol. 102, no. 13, Apr. 2009, Art. no. 135002.
[47] D. Y. Tang, L. M. Zhao, B. Zhao, and A. Q. Liu, "Mechanism of multisoliton formation and soliton energy quantization in passively mode-locked fiber lasers," *Phys. Rev. A*, vol. 72, no. 4, Oct. 2005, Art. no. 043816.
[48] D. Y. Tang, H. Zhang, L. M. Zhao, and X. Wu, "Observation of high-order polarization-locked vector solitons in a fiber laser," *Phys. Rev. Lett.*, vol. 101, no. 15, Oct. 2008, Art. no. 153904.
[49] A. Komarov, H. Leblond, and F. Sanchez, "Quintic complex Ginzburg-Landau model for ring fiber lasers," *Phys. Rev. E.*, vol. 72, no. 2, Aug. 2005, Art. no. 025604.
[50] D. Y. Tang, J. Guo, Y. F. Song, L. Li, L. M. Zhao, and D. Y. Shen, "GHz pulse train generation in fiber lasers by cavity induced modulation instability," *Opt. Fiber Technol.*, vol. 20, no. 6, pp. 610–614, Dec. 2014.
[51] J. Guo, Y. J. Xiang, X. Y. Dai, H. Zhang, and S. C. Wen, "Formation and energy exchange of vector dark solitons in fiber lasers," *IEEE Photon. J.*, vol. 7, no. 1, pp. 1–9, Feb. 2015.
[52] V. V. Afanasjev, P. L. Chu, and B. A. Malomed, "Bound states of dark solitons in the quintic Ginzburg-Landau equation," *Phys. Rev. E.*, vol. 57, no. 1, pp. 1088–1091, Jan. 1998.
[53] S. Coen and T. Sylvestre, "Comment on 'Dark pulse emission of a fiber laser,'" *Phys. Rev. A*, vol. 82, no. 4, Oct. 2010, Art. no. 047801.
[54] D. Y. Tang, L. Li, Y. F. Song, L. M. Zhao, H. Zhang, and D. Y. Shen, "Evidence of dark solitons in all-normal dispersion fiber lasers," *Phys. Rev. A*, vol. 88, no. 1, Jul. 2013, Art. no. 013849.
[55] R. Weill, A. Bekker, V. Smulakovsky, B. Fischer, and O. Gat, "Spectral sidebands and multipulse formation in passively mode locked lasers," *Phys. Rev. A*, vol. 83, no. 4, Apr. 2011, Art. no. 043831.
[56] S. A. Gredeskul and Y. S. Kivshar, "Generation of dark solitons in optical fibers," *Phys. Rev. Lett.*, vol. 62, no. 8, p. 977, Feb. 1989.